ORTHOGONAL VORTEX-ROTOR INTERACTION: IMPACT ON ROTOR CONTROLS, BLADE FLAPPING, THRUST AND POWER

Berend G. van der Wall

berend.vanderwall@dlr.de, German Aerospace Center (DLR, Germany)

Abstract

Rotors of vertical take-off and landing vehicles (main rotor, tail rotor, and propeller) are often subjected to interaction with vortices from other lifting devices. Interactions with vortices whose axes are essentially parallel to the rotor plane of rotation are widely investigated and understood, especially with respect to blade-vortex interaction (BVI) phenomena. Interactions of rotor blades with vortices oriented normal to the rotor disk were rarely investigated and this article focuses on this type of interaction, including the vortex impact on power required by the rotor. It is a fundamental study that is intended to contribute to future flight dynamics investigations.

NOMENCLATURE

C_P	power coefficient
C_T	thrust coefficient
R	helicopter rotor radius, m
r_c	nondimensional vortex core radius
r	nondimensional radial coordinate
V_c	swirl velocity at the core radius, m/s
V_T, V_P	nondimensional tangential and perpendicular velocities at the blade element
x, y, z	nondimensional nonrotating rotor hub coordinates
x_0, y_0	nondimensional vortex position in the rotor disk
Γ, λ_{V0}	Vortex circulation, m²/s, nondimensional vortex circulation
$\overline{L}$	nondimensional blade lift
$\overline{M_\beta}$	nondimensional blade aerodynamic moment about the hub
α_S	shaft angle of attack, deg
$\beta_0, \beta_S, \beta_C$	coning, cyclic rotor blade flapping angles, deg
Δ	perturbation of a variable
γ	Lock number of the rotor blade
$\Theta_0, \Theta_S, \Theta_C$	collective, cyclic rotor blade control angles, deg
Θ_{tw}	blade twist angle per radius, deg
λ	total rotor inflow ratio
λ_i, λ_V	rotor thrust-induced inflow ratio, nondimensional vortex-induced velocity
λ_h	rotor thrust-induced inflow ratio in hover
μ, μ_z	rotor advance ratio, rotor inflow ratio due to disk tilt
σ	rotor solidity
ψ	rotor blade azimuth, deg
Ω	rotor rotational speed, rad/s

1. INTRODUCTION

Rotorcraft interactional aerodynamics has been one of the key research concerns for the design, because they have a great impact on performance, vibration, and aero-acoustic radiation[1],[2]. They are also very important for flight dynamics and handling qualities[3]. Vortex-rotor interactions have a large variety of origins and can come of all sizes and strengths[4]. The most recognized is the blade-vortex interaction (BVI) that leads to strong impulsive noise in descent flight conditions[5]. In this case blade tip vortices that have been generated at the blade tip in the front of the rotor disk travel downstream across the rotor. They are encountered in the aft region of the rotor where the blade leading edge and the vortex axis are parallel to each other. Typical vortex core radii are in the order of 0.5-1% of the rotor radius: $r_c \approx 0.006 - 0.01$.

Another important vortex-rotor interaction occurs when the helicopter is in forward flight and tip

Presented at 44th European Rotorcraft Forum, Delft, The Netherlands, 19-20 September, 2018

vortices generated at the rear position of the main rotor travel downstream into the tail rotor. In this case, the vortices are practically normal to the tail rotor disk as sketched in Fig. 1. The young main rotor blade tip vortices are of size $r_c \approx 0.003$ rotor radius, thus relative to the tail rotor radius, which usually is 1/5 of the main rotor radius, they are of size $r_c \approx 0.027$.

A main rotor ground vortex may also directly affect the tail rotor aerodynamics. Huston[6] sketched that problem, Fig. 2. Again the vortex is normal to the tail rotor disk, and compared to the main rotor tip vortex size this ground vortex has a much larger core diameter. Experimental studies on aerodynamic interactions in hover of main rotor, tail rotor and the airframe have been performed by Balch[7]. One topic was the interaction of the tail rotor with the main rotor regarding main rotor performance aspects. He concludes the best is a wide separation of the rotors and canting the tail rotor.

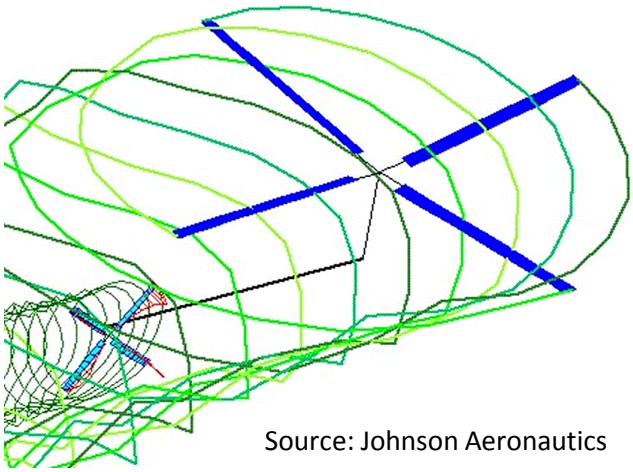

Fig. 1: Sketch of main rotor-tail rotor interaction.

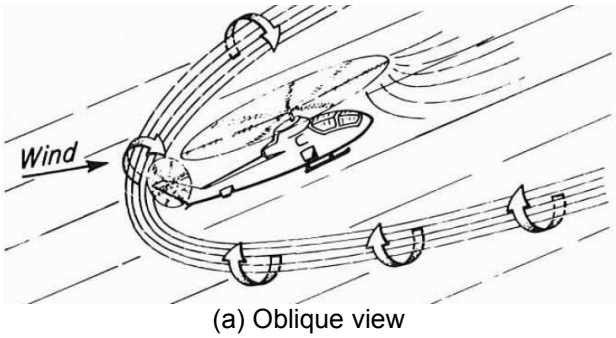

(a) Oblique view

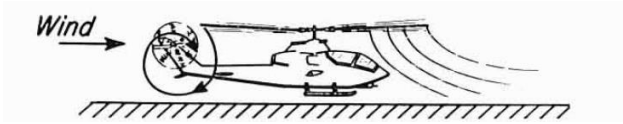

(b) Side view

Fig. 2: Ground vortex-tail rotor interaction[6].

Predictions by means of CFD[8] and particle image velocity measurements[9] of the ground vortex were performed within the EU project HELIFLOW. Vortex core radii in the order of 25% main rotor radius were found ($r_c \approx 0.25$), which represents $r_c \approx 1.25$ for the tail rotor.

Yin and Ahmed[10] applied a panel method combined with free-wake for both main and tail rotors in hover and forward flight for mutual interaction studies. Mainly the tail rotor was subjected to the wake of the main rotor due to its close proximity to it. Contrary, the main rotor was affected by the tail rotor only in hover. A successive wind tunnel test within the EU project HELINOVI aiming at isolated main and tail rotor noise radiation, compared to the combined configuration, included flow velocity measurements on both the suction (denoted PN2 in Fig. 3) and the blowing side (named PN1) of the tail rotor plane[11].

(a) Photo from the starboard side

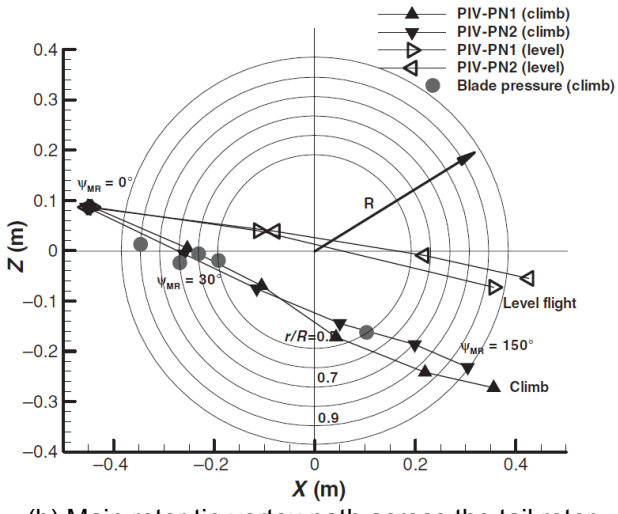

(b) Main rotor tip vortex path across the tail rotor disk, view from port side (wind from left)

Fig. 3: Main rotor/tail rotor interaction in various flight conditions[11].

These measurements identified the main rotor tip vortex trajectories for different level flight and climb conditions across the tail rotor. Their swirl velocity field induced on the tail rotor blades during their passage was measured at different positions, Fig. 3. However, the resolution of the PIV setup was in the

Presented at 44th European Rotorcraft Forum, Delft, The Netherlands, 19-20 September, 2018

order of 2% tail rotor radius and not sufficient to resolve the vortex core radius reliably.

Fletcher and Brown[12] applied the vorticity transport method to a main rotor/tail rotor configuration to investigate aerodynamic interaction effects, computing the isolated rotors first with successive comparison to the combination of both. The tail rotor sense of rotation was investigated also. They found as key aerodynamic factor appears to be that the tail rotor wake undergoes a distinct change in geometry when exposed to the flow field of the main rotor. It is entrained in the main rotor wake by an unsteady process, partly depending on tail rotor sense of rotation. In quartering flight the tail rotor wake and tip vortices travel into the main rotor, Fig. 4.

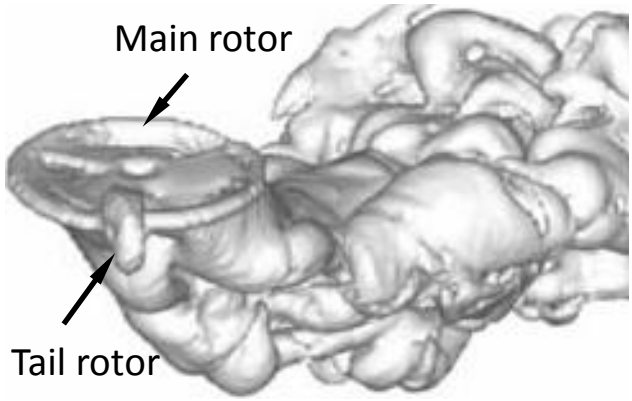

Fig. 4: Wake structure in quartering flight[12].

New mobility concepts include configurations involving wings and propellers. One such concept is the Airbus Helicopters Racer design study as shown in Fig. 5.

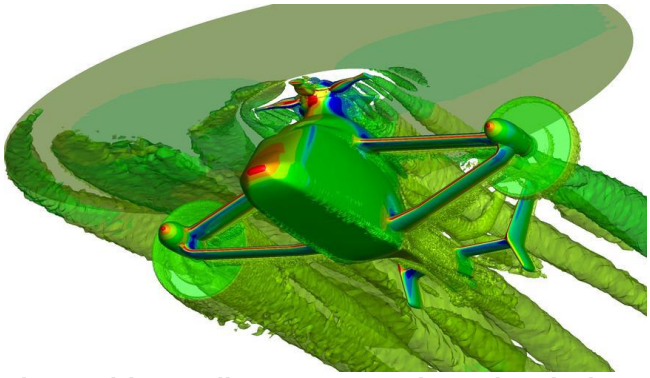

Fig. 5: Airbus Helicopters Racer box wing design with propellers aft of the wing tips, source: DLR.

A part of the investigations is performed within the European Program CleanSky2. A distinct feature of the design is a box wing structure designed to unload the rotor in high-speed flight with nacelles at the outer wing connection and the propeller downstream of the wings. Therefore, the wing tip vortex is centered within the propeller behind them. Such a propeller-vortex interaction and its impact on propeller performance was subject of Yang et al.[13], including wind tunnel tests with flow field measurements, Fig. 6. The vortex core radius was measured with $r_c \approx 0.082$, i.e. 8.2% of the propeller radius.

Finally, helicopters operating in wind farms are also subjected to flight into vortices as sketched in Fig. 7. When flying into the vortex helix at half height, the vortices are normal relative to the main rotor disk and parallel to the tail rotor disk. Contrary, a flight at the top or bottom towards the turbine or away from it is vice versa with respect to the vortex-rotor orientation for both rotors.

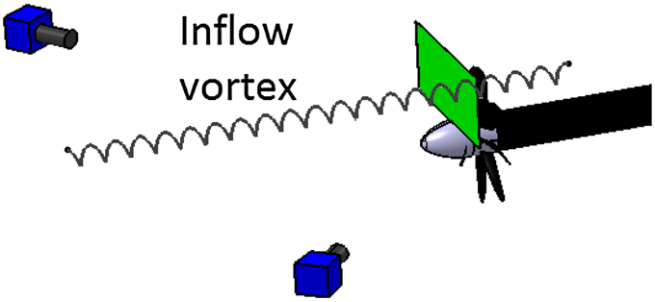

Fig. 6: Arrangement of vortex-propeller measurements[13].

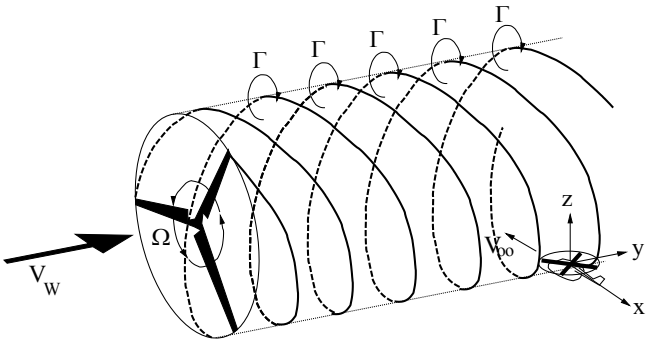

Fig. 7: Wind turbine wake interaction with a helicopter.

The problem of a vortex with its axis parallel to the rotor disk has been investigated intensely in the past and analytical solutions were developed for the rotor controls required to mitigate the vortex effect on thrust and 1/rev flapping moments[14]. Also, the rotor blade flapping that develops when flying into the vortex without pilot action was treated[15]. A preliminary treatment of the orthogonal vortex-rotor interaction and the mathematical method to treat the problem was derived[16]. Regarding the age of the vortex, the core radius ranges from ca. 0.05 m right behind the wind turbine blade tip, about 0.5 m at sufficient distance from the turbine and even more far away. For a helicopter with a rotor radius of about 5 m, this represents core radii in the order of $r_c \approx 0.1$

Presented at 44th European Rotorcraft Forum, Delft, The Netherlands, 19-20 September, 2018

and more. For the tail rotor, 1/5 in size of the main rotor, these core radii are accordingly larger, i.e. $r_c \approx 0.5$ and more.

Atmospheric vortices such as dust devils or small tornadoes have core radii that are of the size of the helicopter's main rotor radius and larger, thus $r_c \geq 1$. All these example confirm that "vortices can come of all sizes and strengths", as stated by McCormick[4].

The subject of this paper is to solve the problem of a vortex with its axis normal to the rotor disk, and to answer the question of how much controls are required to mitigate the effect. Also, how much change of thrust, hub moments and blade flapping will develop when no corrective action is taken.

2. ANALYTICAL TREATMENT

By means of blade element momentum theory the impact of the vortex-induced velocities acting on the rotor blades can be estimated. The velocity components acting at a blade element in tangential (V_T) and perpendicular direction (V_P) are composed of contributions resulting from flight speed, rotor shaft angle of attack, rotor rotation, blade pitch, blade flapping and the mean component of thrust-induced inflow (λ_i), see Fig. 8. Note that in the following all coordinates and lengths are made nondimensional by the rotor radius R, and all velocities by the rotor blade tip speed in hover ΩR.

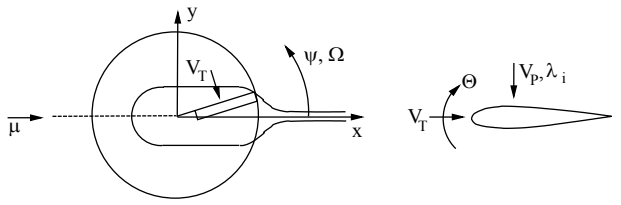

(a) Top view (b) Blade element

Fig. 8: Velocities acting at a blade element of a rotor in undisturbed air.

A rotor trim in undisturbed condition is based on these velocities. In addition, the vortex generates perturbations with its swirl velocity field as sketched in Fig. 9. These are superimposed to the tangential velocities only. A vortex orientation normal to the disk generates induced velocities mainly in the plane of the disk, thus adds to the tangential velocities only ($\Delta V_T \neq 0; \Delta V_P = 0$).

An axial velocity component that is present only inside the vortex core may be considered as well as a velocity perpendicular to the rotor disk, but it is confined to a very small area and quickly decaying after vortex generation[5]. Therefore, this contribution is ignored here. In nondimensional form these velocities include the advance ratio $\mu = V_\infty \cos\alpha_S/(\Omega R)$, $\mu_z = -\mu \tan\alpha_S$:

$$\begin{aligned} V_T &= V_{T0} + \Delta V_T \qquad V_P = V_{P0} + \Delta V_P \\ V_{T0} &= r + \mu \sin\psi \qquad V_{P0} = \mu_z + \lambda_i + r\,d\beta/d\psi \end{aligned} \tag{1}$$

A trim to zero 1/rev flapping eliminates the last term, which is due to rotor blade flapping motion generating a normal velocity at the blades. Next, the perturbations caused by the vortex swirl velocity field are formulated in the following way. From the vortex swirl velocity, only the component adding to the tangential velocity of the blade element of interest is needed. First, the swirl velocity at the blade element at (x, y) induced by a vortex located at (x_0, y_0) is given by Eq. (2), which represents a Vatistas-like swirl velocity profile[17] with a core radius r_c.

$$\begin{aligned} \lambda_V &= \lambda_{V0} \frac{\sqrt{(x-x_0)^2 + (y-y_0)^2}}{(x-x_0)^2 + (y-y_0)^2 + r_c^2} \\ \lambda_{V0} &= \frac{\Gamma}{2\pi\Omega R^2}; \qquad \lambda_{V,\max} = \frac{\lambda_{V0}}{2r_c} \end{aligned} \tag{2}$$

The vortex contribution adding to the blade element tangential velocity is given in Eq. (3). A perturbation in the perpendicular velocity can emerge from rotor thrust variations via the mean induced velocity when no retrim is performed with the vortex included.

$$\begin{aligned} \Delta V_T &= \lambda_V \cos(\psi - \psi_V) \\ &= \lambda_V (\cos\psi \cos\psi_V + \sin\psi \sin\psi_V) \\ &= \lambda_V \frac{|x-x_0| \cos\psi + \mathrm{sgn}(x-x_0)(y-y_0)\sin\psi}{\sqrt{(x-x_0)^2 + (y-y_0)^2}} \\ \Delta V_P &= \Delta\lambda_i + r\,d\beta/d\psi \end{aligned} \tag{3}$$

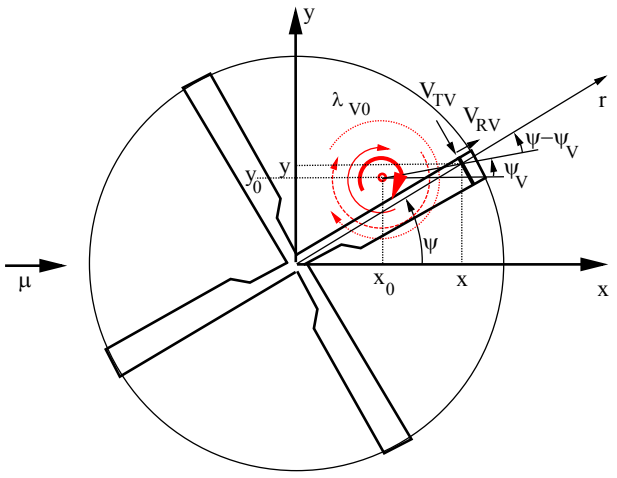

Fig. 9: Vortex velocities acting at a blade element.

The blade pitch consists of the geometric pre-twist (Θ_{tw}, considered as linear here), the pilot inputs: collective, lateral and longitudinal cyclic control

Presented at 44th European Rotorcraft Forum, Delft, The Netherlands, 19-20 September, 2018

angles (Θ_0, Θ_C, Θ_S), and perturbations of these pilot inputs.

$$\begin{aligned}\Theta &= \Theta_0 + \Theta_C \cos\psi + \Theta_S \sin\psi + \Theta_{tw}\left(r - 0.75\right)\\ \Delta\Theta &= \Delta\Theta_0 + \Delta\Theta_C \cos\psi + \Delta\Theta_S \sin\psi\end{aligned} \tag{4}$$

Similarly, blade flapping is decomposed into a part due to trim (coning only) and a perturbation of it (that includes 1/rev flapping motion). A computation of the blade element lift per unit span involves

$$\begin{aligned}V_T^2\left(\Theta + \Delta\Theta - \frac{V_P}{V_T}\right) &= \left(V_{T0} + \Delta V_T\right)^2\left(\Theta + \Delta\Theta\right)\\ &\quad - \left(V_{T0} + \Delta V_T\right)\left(V_{P0} + \Delta V_P\right)\end{aligned} \tag{5}$$

The right side of Eq. (5) can be separated into a fundamental part (a) without perturbations that will be used for trim in undisturbed air and a part (b) including the perturbations that adds to (a) for the case of a trim including the vortex.

$$\begin{aligned}&(a)\quad V_{T0}^2\Theta - V_{T0}V_{P0}\\ &(b)\quad \left(2V_{T0} + \Delta V_T\right)\Delta V_T\Theta + \left(V_{T0} + \Delta V_T\right)^2\Delta\Theta\\ &\qquad - \left(V_{T0} + \Delta V_T\right)\Delta V_P - V_{P0}\Delta V_T\end{aligned} \tag{6}$$

The perturbation part of the sectional lift in Eq. (6) (b) is depending on the trim solution via the pitch angle Θ and via the induced inflow λ_i in V_{P0}. Because Eq. (6) (b) includes a dependency on the trim control angle Θ the controls required to retrim $\Delta\Theta$ are depending on the trim condition. Also, due to the nonlinearity imposed by the term ΔV_T^2 the controls required to retrim $\Delta\Theta$ are depending on the vortex strength in a nonlinear manner.

As example, at zero thrust in undisturbed air Θ in Eq. (4) reduces to the pre-twist and $V_{P0} = 0$. The remainder of Eq. (6) (b) then is

$$\begin{aligned}(b)\quad &\left(2V_{T0} + \Delta V_T\right)\Theta_{tw}(r - 0.75)\Delta V_T\\ &+ \left(V_{T0} + \Delta V_T\right)^2\Delta\Theta - \left(V_{T0} + \Delta V_T\right)\Delta V_P\end{aligned} \tag{7}$$

In this case a vortex will generate some lift and hub moments via the twist and some induced inflow due to the thrust developing. A retrim (to zero thrust) will require some $\Delta\Theta$, because due to the twist the vortex will change the lift locally. For untwisted blades the first term of Eq. (7) (b) vanishes, the pitch will be zero everywhere (due to trim to zero thrust). Then, a retrim thus requires $\Delta\Theta = 0$, because the vortex will modify the dynamic pressure locally, but due to zero pitch this will not generate lift anywhere (only modified drag and thus power). Alternatively, when the rotor is trimmed to its (non-zero) thrust, but no vortex immersed, then $\Delta V_T = \Delta V_P = 0$ and Eq. (6) (b) becomes $V_{T0}^2\Delta\Theta$. Because of the missing vortex perturbation it is obvious that a retrim requires $\Delta\Theta = 0$ (which means that the rotor is already trimmed).

The rotor thrust is based on the mean values of Eq. (6) (a) and (b), and the hub moments are based on the 1/rev cosine and sine part of these expressions. Therefore, a Fourier decomposition is required, of which only the mean value and the 1/rev coefficients are needed. For (a) this is easily done, ignoring higher harmonic terms in 2/rev and 3/rev that do not contribute to the steady rotor trim.

$$\begin{aligned}V_{T0}^2\Theta - V_{T0}V_{P0} &= \left(r + \mu\sin\psi\right)^2\\ &\quad\times\left[\Theta_0 + \Theta_C\cos\psi + \Theta_S\sin\psi + \Theta_{tw}(r - 0.75)\right]\\ &\quad - \left(r + \mu\sin\psi\right)\left(\mu_z + \lambda_i + r\,d\beta/d\psi\right)\end{aligned} \tag{8}$$

The Fourier decomposition of Eq. (6) (b) in analytical form cannot be derived directly due to the broken rational function in Eq. (3) which describes the vortex contribution. Note that therein the following substitutions have to be made:

$$x = r\cos\psi; \qquad y = r\sin\psi \tag{9}$$

Therefore, the Fourier analysis and the resulting spanwise integrals over the radial coordinate needed for thrust and hub moments are evaluated numerically with a 1 deg resolution in azimuth and with a radial resolution of $\Delta r = 0.02$ in order to resolve vortices with core radii down to $r_c \geq 0.02$. The nondimensional blade lift and aerodynamic moment about the hub are derived[18], and the integral's argument is given in Eq. (5).

$$\begin{aligned}\bar{L} &= \int_A^B \overline{dL} \approx \frac{1}{2}\int_A^B V_T^2\left(\Theta + \Delta\Theta - \frac{V_P}{V_T}\right)dr\\ \overline{M_\beta} &= \int_A^B r\,\overline{dL}\end{aligned} \tag{10}$$

3. RESULTS

A rotor trim of the isolated rotor in undisturbed condition is performed first and employs collective Θ_0, lateral cyclic Θ_C and longitudinal cyclic Θ_S controls in order to trim to the desired thrust coefficient C_T, propulsive force via tilting the rotor by the shaft angle, and to desired hub moments. For simplicity a central blade hinge is assumed without flapping motion in 1/rev, i.e., the tip path plane is perpendicular to the rotor shaft. Steady 2D aerodynamics are used, the rotor blade has a root cutout of 25% radius and an effective aerodynamic end at 97% radius, accounting for tip losses.

Presented at 44th European Rotorcraft Forum, Delft, The Netherlands, 19-20 September, 2018

The example used here is a Mach-scaled 2.300 kg Bo105 helicopter. A trim to a specific blade loading of $C_T/\sigma = 0.0731$ with a solidity of $\sigma = 0.077$ has been performed on a 4-bladed model-scale rotor with a radius of $R = 2$ m and a tip speed of $\Omega R = 218$ m/s. Rotor trim versus flight speed, based on lift and propulsive force of the isolated rotor, is shown in Fig. 10.

The lateral cyclic control angle is zero throughout the speed range because a constant inflow without a longitudinal gradient is employed. The total inflow increases with flight speed due to nose-down tilt of the rotor, while the induced inflow asymptotically decreases. Although the assumption of a constant inflow is a crude approximation in general, here it is justified because here the trim is just an initial condition, and the interesting part is any vortex influence *relative* to this trim condition.

The nondimensional vortex circulation strength was set to $\lambda_{V0} = 0.01$ and 0.02 (this represents a circulation of $\Gamma = 27$ and 55 m²/s, respectively, and is considered as representative for mid-size wind turbines[18]) and its core radius to $r_c = 0.1$, which leads to a maximum swirl velocity of $\lambda_{V,max} = 0.05$ and 0.1, which is 5% and 10% of the blade tip speed, respectively. The vortex sense of rotation is opposite to that of the rotor blades.

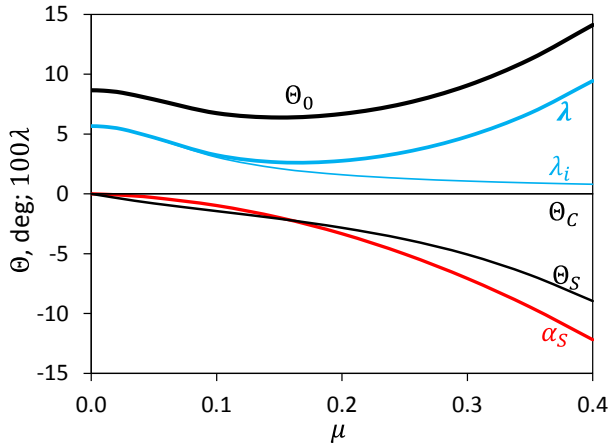

Fig. 10: Rotor controls and induced inflow for a trim to constant thrust and zero hub moments.

3.1. The rotor in hover

First, the retrim of the rotor with a vortex included is performed in hover, i.e. for $\mu = 0$. The vortex locations are varied along the centerline of the rotor in the range $-3 \le y_0 \le +3$ and the rotor is retrimmed. $y_0$is the vortex center position relative to the hub center, nondimensionalized by the rotor radius. The needed perturbation control angles to retain trim are shown in Fig. 11.

Two different vortex strengths of $\lambda_{V0} = 0.01$ and 0.02 were investigated; the nondimensional core radius is $r_c = 0.1$. In Fig. 11 (a) the control angles are given in physical units, in (b) they are normalized by the vortex strength. In this operational condition the controls required to retrim the rotor are practically linear depending on the vortex strength and the nonlinearity $\Delta V_T^2 \Theta$ indicated in Eq. (6) (b) can be neglected in this condition.

Collective control angle Θ_0: when the vortex is outside the rotor disk its impact on rotor thrust and thus the collective control angle is negligible. For vortex positions inside the disk the influence on rotor thrust and collective becomes stronger and the maximum is reached when the vortex is located in the hub center.

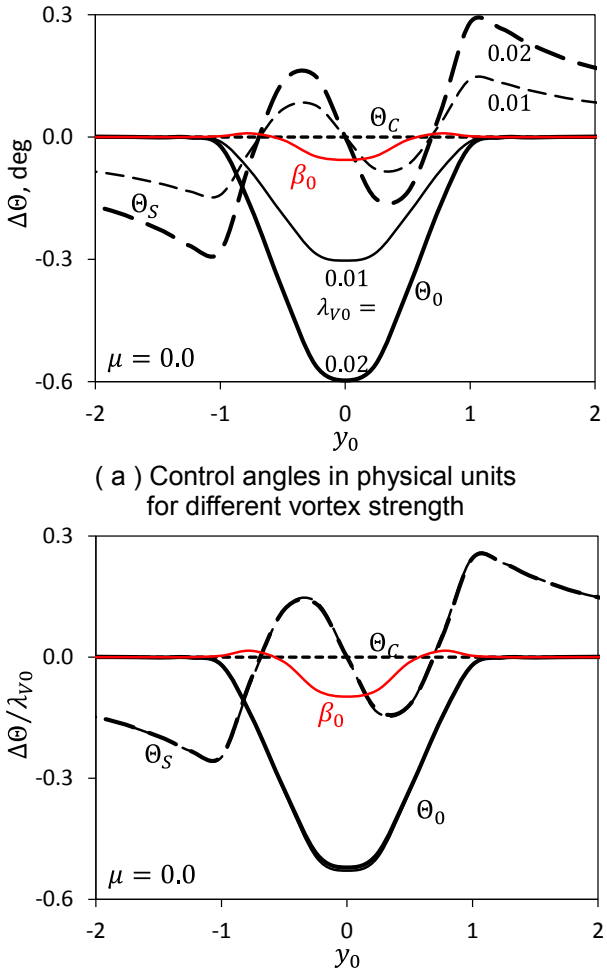

(a) Control angles in physical units for different vortex strength

(b) Control angles referred to the vortex strength

Fig. 11: Controls required to retrim the rotor in hover.

The physical reason is that in a center position it introduces additional tangential velocities everywhere in the rotor disk, thus increasing the dynamic pressure all over and consequently increasing rotor thrust, as is shown in Fig. 12. Also,

Presented at 44th European Rotorcraft Forum, Delft, The Netherlands, 19-20 September, 2018

the stronger the vortex, the larger the collective required to retrim the rotor. The vortex impact on local dynamic pressure is largest when it is close to the blade tip, because the blade rotational velocity is largest there. In vicinity of the rotor hub the blade circumferential velocity is small, thus the change of dynamic pressure due to the vortex is smaller as well.

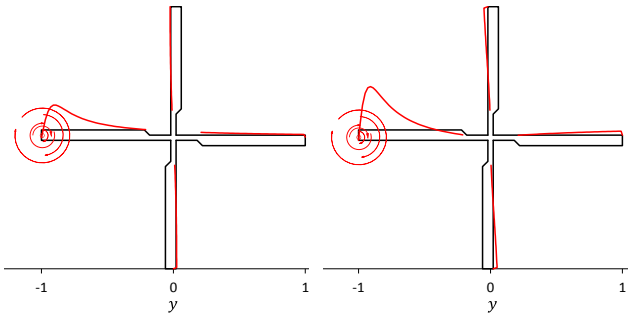

(a) velocity induced, $y_0 = -1$ (b) dynamic pressure

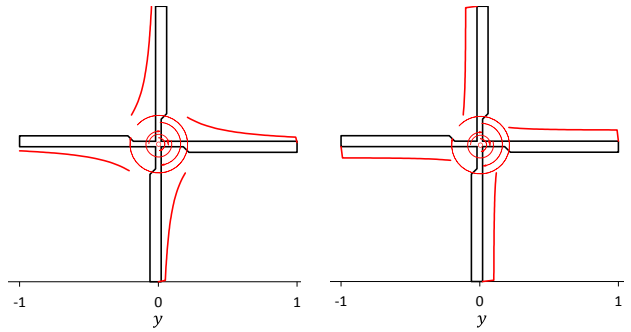

(c) velocity induced, $y_0 = 0$ (d) dynamic pressure

Fig. 12: Vortex-induced velocities on the rotor blades, hover.

The nondimensional tangential velocity V_T and the total dynamic pressure $V_T|V_T|$ distributions along the radial direction in hover are shown in Fig. 13 for a vortex position in the hub center. The thin lines denote the distributions without a vortex, the thick lines including the vortex. Due to the vortex influence the tangential velocity is not increasing linear; the maximum nondimensional vortex swirl velocity at its core radius (0.1 rotor radius) is clearly visible.

At the blade tip the swirl velocity is significantly smaller due to the induced velocity profile of Eq. (2), while the nondimensional circumferential velocity of rotor rotation is maximum there, both summing up to a value of 1.01. Within the dynamic pressure distribution the vortex influence is not that much visible, but at the blade tip the remaining vortex-induced velocity causes the dynamic pressure to have a value slightly over 1 (1.02 actually). Overall an increase of dynamic pressure is visible and a retrim to the same thrust requires some control angle perturbations that eliminate the consequences of the dynamic pressure on rotor thrust and aerodynamic hub moments.

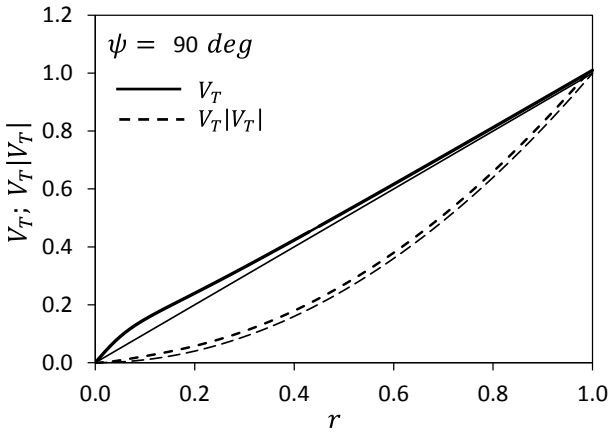

Fig. 13: Distribution of tangential velocity and dynamic pressure, hover. $\lambda_{V0} = 0.01$, vortex in the hub center.

Longitudinal cyclic control angle Θ_S: When the vortex approaches the rotor from the left side ($y_0 < -1$ in Fig. 11 (b)) it generates rearward velocities to the revolving blades in the left (retreating) side of the rotor and increased tangential velocities in the right (advancing) side of the rotor. This leads to a loss of lift in the left region and an increase of lift in the right part. Therefore the longitudinal control angle must be negative to eliminate that unbalance. This changes quickly once the vortex entered the rotor disk and turns to the opposite at a position of $y_0 \approx -0.77$.

Inside that range the maximum positive longitudinal control angle is found at $y_0 \approx -0.4$. At this position the vortex increases the lift on the left of the rotor more than on the right, requiring a positive control angle to eliminate this unbalance. At the center position the vortex generates a rotational symmetric flow field in the rotor disk and no unbalance between left and right exists, thus the control angle is zero. Finally, when the vortex is placed in the right part of the rotor, its impact on left and right lift distribution is mirrored compared to vortex positions in the left.

Lateral cyclic control angle Θ_C: For all vortex positions the lateral control angle perturbations remain zero (see Fig. 11 (b)), because in longitudinal direction all disturbances of lift are symmetric and thus no unbalance exists.

When placing the vortex along the centerline in longitudinal direction, the results for the longitudinal and lateral control angles simply exchange, while the result for the collective control remains the same.

Presented at 44th European Rotorcraft Forum, Delft, The Netherlands, 19-20 September, 2018

Rotor coning β_0: The red line in Fig. 11 (b) gives the result for $\lambda_{V0} = 0.01$ only. Despite retrimming the rotor to constant thrust some mean flapping results from a radial redistribution of the mean section lift, which is largest for a central vortex position. In this case the dynamic pressure is increased everywhere in the rotor disk, and the negative collective applied to maintain thrust constant reduces the blade lift mainly at the blade tip area. This has a dominant effect on shifting the center of lift more inboard, thus reducing the aerodynamic moment about the hub and with it the blade coning angle.

This is illustrated in Fig. 14, giving the radial distribution of lift and the radial position of the mean lift for a vortex position in the hub center. The increased dynamic pressure due to the vortex influence is compensated by a reduced collective control angle (Fig. 11), which dominates at the blade tip region to reduce loading there. Inboard of about 0.65 radius the vortex-induced increase of dynamic pressure dominates the change of collective control and increases the lift there.

The total lift remains constant, but the center of lift is slightly moving inboard, from 0.749 to 0.737 radial position, and the aerodynamic moment about the hub is reduced proportionally. Consequently, the rotor coning is as well reduced accordingly, as seen in Fig. 11.

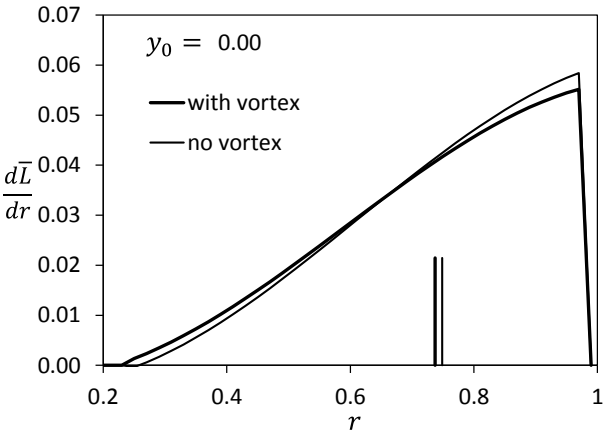

Fig. 14: Lift distribution in hover. $\lambda_{V0} = 0.01$, vortex in the hub center.

3.2. Forward flight

In forward flight the asymmetry of dynamic pressure on the advancing and the retreating side become effective. Results are shown for an advance ratio of $\mu = 0.3$ in Fig. 15, and are compared to the hovering case shown before to highlight the relative differences. Now a retrim of the thrust requires a specific combination of collective and longitudinal cyclic control angles, because both affect the rotor thrust and the aerodynamic rolling moment.

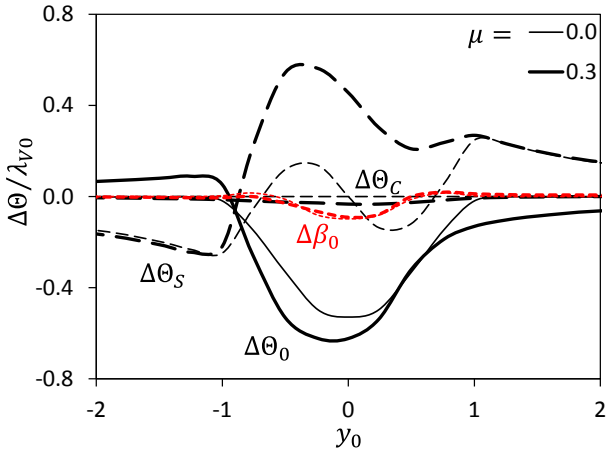

Fig. 15: Controls required to retrim the rotor in forward flight.

Collective control angle Θ_0: the overall character of collective control angle required for retrim is similar to the hovering case, but with larger magnitude because of an increased average dynamic pressure acting on the blades. In contrast to hover, vortex positions on either sides outside the disk already require some collective control as well due to the longitudinal cyclic, which now affects the thrust.

Longitudinal cyclic control angle Θ_S: As long as the vortex remains outside the rotor disk results differ only marginally from the hovering case. For vortex positions inside the disk, however, the longitudinal control angle is affected by two parts: one due to the vortex disturbance similar to that in hover, and another one do compensate the collective control angle impact on the aerodynamic rolling moment. The latter, due to a negative collective control angle, causes a positive longitudinal control angle and thus the curve is positive for almost all vortex positions inside the rotor disk.

Lateral cyclic control angle Θ_C: while zero in hover, a very small lateral cyclic control angle is required in forward flight for retrimming the hub aerodynamic pitching moment. Due to its small magnitude its effect is considered negligible.

Rotor coning β_0: The red line in Fig. 15 indicates the rotor coning developing due to radial redistribution of the mean lift. In forward flight a small asymmetry is visible relative to the hovering case, but this is a marginal difference. In general the effect is essentially the same as in hover.

Because the source of trim modifications lies in the modified dynamic pressure, which is the square of the tangential velocities, the vortex influence becomes more nonlinear in forward flight than in hover. The difference in local dynamic pressure caused by the vortex is shown qualitatively in Fig. 16

Presented at 44th European Rotorcraft Forum, Delft, The Netherlands, 19-20 September, 2018

for vortex positions at the tip of the retreating blade, at the center of the rotor and at the tip of the advancing side.

The vortex strength is constant throughout, thus its induced velocities are constant as well. Its influence on dynamic pressure, however, is much weaker on the retreating side than on the advancing side. This is due to the square of V_T in the dynamic pressure, introducing a term $2V_{T0}\Delta V_T$ which is smaller on the retreating side than on the advancing side, because $V_{T0} = r + \mu \sin\psi$, see Eq. (1). On the advancing side $\psi = 90°$ and the second term is positive, while on the retreating side $\psi = 270°$ and the second term is much smaller, or even negative for $r < \mu$.

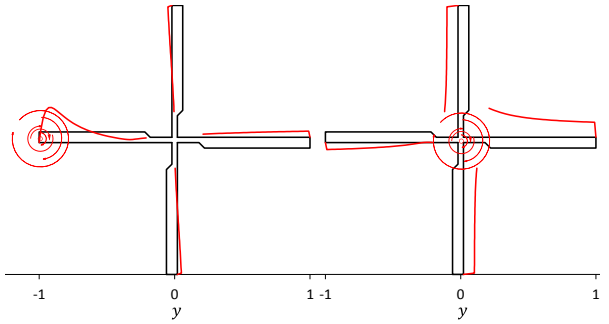

(a) $y_0 = -1$ (b) $y_0 = 0$

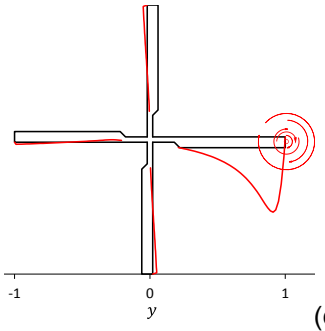

(c) $y_0 = 1$

Fig. 16: Vortex-induced dynamic pressure on the rotor blades, $\mu = 0.3$.

3.3. Vortex impact on thrust and flapping in case of no retrim

If no retrim is performed, the vortex – due to its influence on the dynamic pressure distribution (see Fig. 13) – will change the rotor thrust and accordingly the rotor blade flapping. The undisturbed trim is performed for zero blade flapping, thus any flapping developing is due to the vortex influence. For a hovering case with the vortex in the hub center the resulting lift distribution is shown in Fig. 17. Over the entire span of the blade length the lift is higher than in the trimmed undisturbed case with a slightly larger increment inboard than outboard. This generates more thrust and shifts the center of lift little more inboard. The aerodynamic moment about the hub center is thus increased, and with it the blade coning will increase as well relative to the undisturbed trim condition. Results are given in Fig. 18. A Lock number of $\gamma = 8$ has been used here, and as the blade flapping response is always proportional to the Lock number, thus different values will lead to proportionally different results.

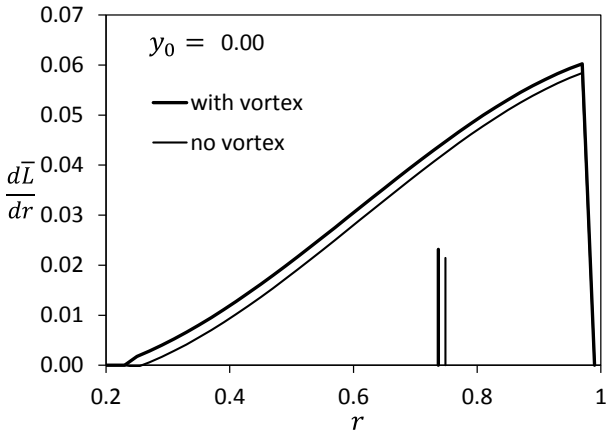

Fig. 17: Lift distribution without retrim in er. $\lambda_{V0} = 0.01$, vortex in the hub center.

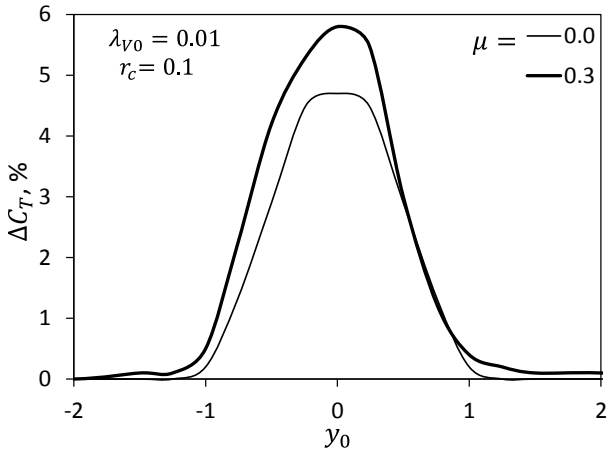

(a) Thrust increase due to vortex influence

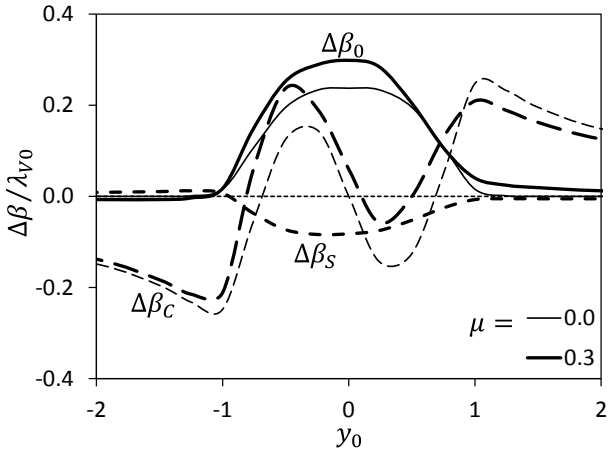

(b) Rotor flapping due to vortex influence

Fig. 18: Vortex impact on thrust and blade flapping in case of no retrim.

Presented at 44th European Rotorcraft Forum, Delft, The Netherlands, 19-20 September, 2018

Rotor thrust coefficient C_T *and Rotor coning* β_0: When no (negative) collective control angle is employed to eliminate the increase of thrust due to the vortex impact on lift, then the overall thrust increases, see Fig. 18 (a), and accordingly the blade coning (b). In forward flight the increase is a little stronger than in hover because the average dynamic pressure is increasing. An asymmetry is also developing with flight speed, generating more lift when the vortex is on the retreating side of the rotor. This is because in that case the vortex-induced velocity adding to the advancing side with its already increased dynamic pressure due to flight speed is more effective than adding to the lower dynamic pressure on the retreating side when the vortex is on the advancing side.

Longitudinal blade flapping angle β_C: Because the longitudinal control angle Θ_S now does not eliminate the aerodynamic hub rolling moment now the longitudinal blade flapping develops in the same manner.

Lateral blade flapping angle β_S: While zero in hover, in forward flight a little amount of lateral blade flapping develops, similar to the lateral control angle Θ_C in forward flight, which is not employed now. Relative to the coning and longitudinal flapping, however, this lateral flapping is of minor importance.

3.4. Vortex impact on rotor power

Rotor power is affected in two ways. First, whether retrimmed or not, the increase or reduction of local dynamic pressure modifies the local airfoil drag and as well the angle of attack, leading to a different lift coefficient, and thus to a different induced drag. Second, in case of no retrim, the overall thrust will vary and with it the rotor induced inflow, therefore the overall induced power will be modified.

The sense of rotation also plays a role in forward flight, because despite the in-plane velocities add linearly, the resulting dynamic pressure – the square of the resulting velocities – will be nonlinear. In case of retrimming the rotor the overall thrust remains constant, thus the global induced velocity as well, and only the local effects are remaining.

The variation of rotor power, depending on the vortex position as before, is given in Fig. 19 for $\lambda_{V0} = 0.01, r_c = 0.1$. Results for hover and $\mu = 0.3$ are shown.

The major impact of the vortex is obtained when it is inside the rotor disk, and the maximum obtained for a position in the rotor center. In this case all blades are affected by increased dynamic pressure due to the vortex.

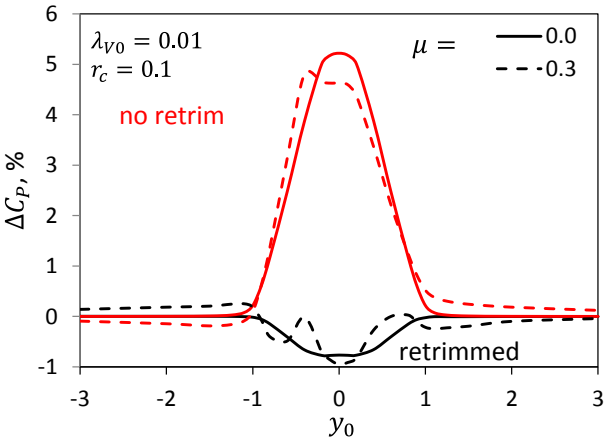

Fig. 19: Vortex impact on rotor power in hover and forward flight.

In the case of retrim this requires less collective control, hence less angle of attack, and thus the induced drag is reduced as well. This effect is larger than the increase in airfoil drag due to the larger dynamic pressure. However, the power reduction is merely 1% relative to the trim in undisturbed air for this vortex strength and size.

If no retrim is performed, the thrust is increasing due to the increase of dynamic pressure at the blades (see Fig. 18 (a)), thus the mean induced inflow and with it the overall induced power, in addition to the increase of airfoil power. This results in an increase of 5% of rotor power relative to the undisturbed trim for this combination of vortex strength and size. The influence of the advance ratio is relatively small, it shifts the curves slightly to vortex positions more on the retreating side for this sense of vortex rotation.

Next, the influence of vortex strength and sense of rotation is the subject of discussion, shown in Fig. 20 for a range of vortex strengths λ_{V0} ranging from -0.08 to +0.08; the peak induced velocity at the vortex core radius is reaching 40% of the rotor tip speed in these extreme cases. In this case the vortex can cause reversed flow in the inner portions of the rotor disk, i.e. for $r \leq 0.4$, but can also increase the tangential velocities there to more than the tip speed of the rotor.

When the vortex core is at the blade tip, it can locally reduce the effective tangential velocity to 20% of the tip speed, or increase it to 140%. However, it must be mentioned that no compressibility effects are accounted for in this study.

In case of retrim (black curves) a clockwise sense of vortex rotation ($\lambda_{V0} > 0$) adds to the tangential velocities of the blades, increases the dynamic pressure, and – as explained before – reduces the overall power, in maximum for the cases investigated here by almost 7%. The opposite sense

Presented at 44th European Rotorcraft Forum, Delft, The Netherlands, 19-20 September, 2018

of rotation reduces the dynamic pressure at the blades, thus increases the inflow angles, requires more collective control to retrim the thrust, and results in about 5% more power required.

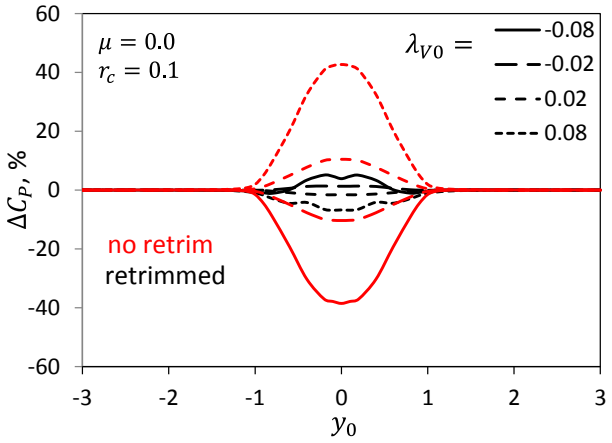

Fig. 20: Influence of vortex strength and sense of rotation on rotor power in hover.

In case of no retrim the rotor thrust undergoes large variations and the additional global inflow associated with the thrust significantly affects the rotor power. In case of the clockwise rotating vortex ($\lambda_{V0} > 0$) the dynamic pressure is increased, thus the thrust is increased, and the power goes up by 42%, while the opposite sense of rotation reduces the power by up to 38%. The different extremal values in case of retrim and no retrim indicate the nonlinearity of the problem.

Finally, a comparison with an executed experiment is given and the parameters of the setup are taken from Yang et al.[13]; see also Fig. 6. The parameters of the propeller, its operational condition, and the vortex parameters are given in Table 1.

Table 1: Parameters of Yang's experiment

Rotor data:

N_b	R, m	σ	ΩR, m/s	$C_{l\alpha}$	Θ_{tw}, deg
4	0.152	0.586	101.9	5.5	-32

Operational condition and vortex data:

V_∞, m/s	C_T	C_P	y_0	r_c	$\lambda_{V0,max}$
19.2	0.0733	0.0387	0.75	0.082	0.023

They performed experiments with the propeller in undisturbed air first, then inserting a semi-span wing as vortex generator upstream into the wind tunnel test section with different angles of attack such that the vortex sense of rotation and strength up to the maximum values as given in Table 1 could be varied. No retrim was done for the propeller, but the variation of thrust and power was measured. Fig. 21 compares experimental results obtained from Yang et al.[13] with those computed by the model presented here. Both the vortex strength and its sign of rotation were varied in the experiment and propeller thrust and power were measured without the vortex first, then with the vortex impinging the propeller. Note that the sign definition for vortex sense of rotation relative to that of the propeller sense of rotation in the experiment was opposite to that used in this paper.

Thrust and power changes have been predicted by the analytical model of this paper. The overall trend of the experimental data is well captured by the model, confirming the principal validity of the approach. The model predicts a little stronger vortex impact on thrust changes than on power changes.

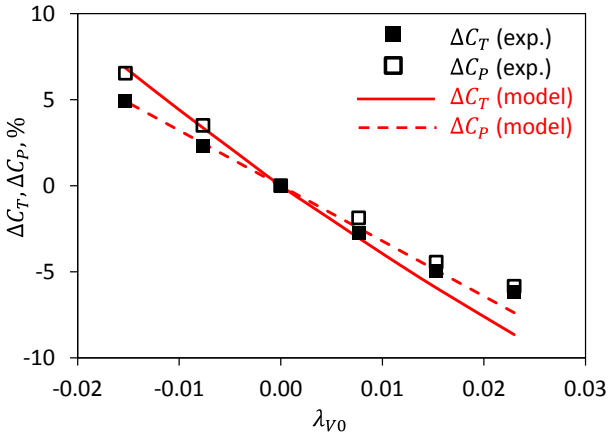

Fig. 21: Influence of vortex strength and sense of rotation on propeller thrust and power in hover for data from Yang at al.[13].

4. CONCLUSIONS

- A vortex-rotor interaction with a vortex axis normal to the rotor disk causes local disturbances that change the tangential velocity field at the blade elements in a very nonlinear manner.
- The compensation of these disturbances with collective and cyclic control angles is possible with moderate magnitudes of control angles. Compared to results obtained for vortex-rotor interactions where the vortex is lying planar in the disk[14],[15], the rotor controls required to retrim the rotor of a vortex normal to the disk are much smaller. However, the stronger the vortex, the larger the controls required until the control limits are achieved.
- With no controls employed, the vortex impact on rotor thrust and hub moments causes rotor blade flapping response in coning and cyclic flapping angles. The response is essentially proportional to the vortex strength and to the Lock number of the blades.
- In forward flight, due to an average increase of dynamic pressure, the controls required for retrimming the rotor increase over the values

Presented at 44th European Rotorcraft Forum, Delft, The Netherlands, 19-20 September, 2018

obtained in hover, especially in longitudinal control, which then is required to mitigate the direct impact of the vortex, and also to mitigate the influence of the collective control on the aerodynamic rolling moment. With no controls employed in forward flight, the blade flapping also increases in magnitude over the values obtained in hover.

- When retrimmed to the operating condition in undisturbed air the power required increases or decreases by a small amount (few %) only, depending on vortex strength and sense of rotation relative to the rotor sense of rotation. If no retrim is performed, rotor thrust and power changes can be very substantial.
- A comparison with data of an executed wind tunnel test confirms the validity of this approach.

Although this study is a fundamental phenomenological study only it is intended to contribute to future flight dynamics investigations that may also aim to identify potential hazardous conditions.

5. REFERENCES

[1] Sheridan, P.F., and Smith, R.P., "Interactional Aerodynamics – a New Challenge to Helicopter Technology," Journal of the American Helicopter Society, Vol. 25, (1), 1980, pp. 3-21.

[2] Huber, H., and Polz, G., "Studies on Blade-to-Blade and Rotor-Fuselage-Tail Interferences," *Aircraft Engineering and Aerospace Technology*, Vol. 55, (10), 1983, pp. 2-12.

[3] Padfield, G.D., "Helicopter Flight Dynamics," Reston, VA: American Inst. of Aeronautics and Astronautics, 2007.

[4] McCormick, B.W., "Hurricanes, Tornadoes, Wake Turbulence and BVI – Vortices Come in all Sizes," Journal of the American Helicopter Society, Vol., 50, (3), 2005, pp. 219-229.

[5] Leishman, J.G., "Principles of Helicopter Aerodynamics," Cambridge University Press, Cambridge, 2000.

[6] Huston, R.J., Morris, C.E.K., "A Note on a Phenomenon Affecting Helicopter Directional Control in Rearward Flight," Journal of the American Helicopter Society, Vol. 15, (4), 1970, pp. 38-45.

[7] Balch, D.T., "Experimental Study of Main rotor/Tail Rotor/Airframe Interaction in Hover," Journal of the American Helicopter Society, Vol. 30**,** (2), 1985, pp. 49-56.

[8] Boer, J.F., "HELIFLOW Task 3 Ground Vortex Pre-Test Calculations," NLR-TR-98578 (HELIFLOW/3/NLR/01A), Amsterdam, Netherlands, 1998.

[9] Pengel, K., and Mercker, E., "Improved Experimental and Theoretical Tools for Helicopter Aeromechanic and Aeroelastic Interactions, Task 3: Sideward Flight Tests, Subtask 3.3: Test Conduct, Deliverable 3-9: Report on the Particle Image Velocimetry Data," Report HFLOW/3/DNW/09, Nordoostpolder, Netherlands, 2001.

[10] Yin, J., Ahmed, S.R., "Helicopter Main-Rotor/Tail-Rotor Interaction," Journal of the American Helicopter Society, Vol. 45, (4), 2000, pp. 293-302.

[11] Yin, J., van der Wall, B.G., Oerlemans, S., "Acoustic Wind Tunnel Tests on Helicopter Tail Rotor Noise (HeliNOVI)," Journal of the American Helicopter Society, Vol. 53, (3), 2008, pp. 226-239.

[12] Fletcher, T.M., Brown, R.E., "Main Rotor-Tail Rotor Interaction and its Implications for Helicopter Directional Control," Journal of the American Helicopter Society, Vol. 53, (2), 2008, pp. 125-138.

[13] Yang, Y., Zhou, T., Sciacchitano, A., Veldhuis, L, Eitelberg, G., "Propeller and Inflow Vortex Interaction: Vortex Response and Impact on the Propeller Performance," *CEAS Aeronautical Journal*, Vol. 7, (3), 2016, pp. 419-428.

[14] van der Wall, B.G., van der Wall, L.B., "Analytical Estimate of Rotor Controls Required for a Straight Vortex Disturbance Rejection," Journal of the American Helicopter Society, Vol. 62, (1), 2017, pp. 015001-1-4.

[15] van der Wall, B.G., "Analytical Estimate of Rotor Blade Flapping Caused by a Straight Vortex Disturbance," Journal of the American Helicopter Society, Vol. 62, (4), 2017, pp. 045001-1-6.

[16] van der Wall, B.G., "Estimate of Rotor Controls and Blade Flapping Caused by an Orthogonal Vortex Disturbance," Journal of the American Helicopter Society, Vol. 63, (2), 2018, pp. 025000-1-6.

[17] Vatistas, G.H., Kozel, V., Mih, W.C., "A Simpler Model for Concentrated Vortices," *Experiments in Fluids*, Vol. 11, (1), 1991, pp. 73-76.

[18] van der Wall, B.G., Fischenberg, D., Lehmann, P.H., van der Wall, L.B., "Impact of Wind Energy Rotor Wakes on Fixed-Wing Aircraft and Helicopters," 42nd European Rotorcraft Forum, Lille, France, Sept. 5-8, 2016.

Presented at 44th European Rotorcraft Forum, Delft, The Netherlands, 19-20 September, 2018